GSA Data Repository 2018363

Sub-arc xenolith Fe-Li-Pb isotopes and textures tell tales of their journey through the mantle wedge and crust

Simon Turner, Helen Williams, Janne Blichert-Toft, Sandra Piazolo, Mitchel Gerdes, John Adam, Xiao-Ming Liu, Bruce Schaefer and Rene Maury

This data supplement includes Tables DR1-4 in Excel format.

Analytical Methods

Quantitative orientation analysis (Electron back-scatter diffraction) was performed at Macquarie Geoanalytical using the Carl Zeiss IVO SEM at 20kV, high vaccum and 8.0 nA. Patterns were acquired with HKL NordlysNano high sensitivity EBSD detector and indexed using AzTec analysis software (Oxford Instruments). Analyses were acquired on a raster grid with step sizes of 4-10 mm. Post-acquisition analysis was performed using the Channel 5 software (Oxford Instruments) using a "standard" noise reduction (Piazolo et al., 2006). Grain boundaries are defined as areas surrounded by 10º boundaries, while sub-grain boundaries have misorientations less than 10º. Mineral analyses were obtained using a Cameca SX100 with an accelerating voltage of 15 keV and a focused beam current of 20 nA. A defocussed beam was used to measure the groundmass of the host lava. A counting time of 10 seconds was assigned to both peak and background measurements. Spectrometer calibration was achieved using the following standards: Jadeite (Na), Fayalite (Fe), kyanite (Al), olivine (Mg), chromite (Cr), spessartine garnet (Mn), orthoclase (K), wollastonite (Ca, Si) and TiO_2 (Ti). Mineral trace element analyses were performed in situ using a Photon Machines Excite 193 Eximer laser coupled to an Agilent Technologies 7700 Series quadrupole inductively-coupled plasma mass spectrometer, Glitter software and NIST610 Glass as a calibration standard and BHVO-2G and BCR-2G as reference materials.

The whole rock isotope analyses of the harzburgites reported in Table DR1 were obtained on splits of the same powders used in Turner et al. (2012). Boron isotopic composition was determined at the Istituto di Geoscienze e Georisorse, Pisa, by the dicesium borate method using a VG Isomass 54E positive thermal ionization mass spectrometer, following separation of boron by ion-exchange procedures (Tonorini et al., 1997). Total procedural blanks (8-12 ng) are negligible relative to the amount of sample processed. Correction for isotopic fractionation associated with mass spectrometric analysis was made using a fractionation factor (including correction for ^{17}O

contributions), calculated as {(R_{cert}+0.00079)/R_{meas}}, relative to NIST SRM 951 (R_{meas} = $^{11}B/^{10}B_{meas}$ = 4.0498±0.0010). An aliquot of this standard was processed identically with each batch of samples. Boron isotopic composition is reported in conventional delta notation ($\delta^{11}B$) as per mil (‰) deviation from the accepted composition of NIST SRM-951 (R_{cert} = 4.04362). Long-term reproducibility of isotopically homogeneous samples treated with alkaline fusion chemistry is approximately ± 0.5‰ and replicate analyses of all samples agree within this limit. Accuracy was evaluated independently via multiple analyses of the GSJ-JB2 basalt reference standard, for which we obtained an average $\delta^{11}B$ of 7.13 ± 0.19‰ ($2\sigma_{mean}$; n = 17).

Samples (and standards) were prepared for Li isotopic analysis at the University of Maryland by digesting the powders with a 3:1 mixture of concentrated HF and HNO_3 in Savillex® screw top beakers on a hot plate (T~ 90°C). This was followed by addition of HNO_3 and HCl, with drying between each stage of acid addition. The residue was then re-dissolved in 4 M HCl in preparation for four-column ion-exchange chromatography (Rudnick et al., 2004). For each column, 1 ml of cation exchange resin of AG50w-X12, 200-400 mesh (Bio-Rad) was cleaned with HCl and Milli-Q water followed by conditioning, chemical separation and sample collection using an eluent mixture of HCl and ethanol. The first two columns remove major element cations with 2.5M HCl and subsequently 0.15M HCl. The third and fourth columns separate Na from Li with 30% ethanol in 0.5M HCl through a N_2 pressurized ion exchange column (Rudnick et al., 2004). The samples were analyzed for ^6Li and ^7Li on a Nu Plasma multiple-collector inductively coupled plasma mass spectrometer using faraday cups. Li isotopic compositions were analyzed by bracketing the sample, before and after, with the L-SVEC standard. The δ^7Li value (δ^7Li =[[$^7Li/^6Li]_{sample}$ / [$^7Li/^6Li]_{standard}$ – 1 x 1000]) is expressed as per mil deviations from the LSVEC standard. External reproducibility of the isotopic compositions is ≤ ±1.0‰ (2σ) based on repeat runs of pure Li standard solutions: in-house standard UMD-1 and international standard reference material IRMM-016.

Iron isotopic analyses followed procedures described in Williams and Bizimis (2014) using a ThermoFisher Neptune multiple-collector inductively coupled plasma mass spectrometer at the University of Durham. Instrumental mass bias was corrected for by sample–standard bracketing where the sample and standard Fe beam intensities (typically 35–40V ^{56}Fe for a standard 10^{11} resistor) were matched to 5%. Mass dependence, long-term reproducibility and accuracy were evaluated by analysis of an in-house FeCl salt standard ($\delta^{57}Fe$ = −1.06 ± 0.07‰; $\delta^{56}Fe$ = −0.71 ± 0.06‰ 2S.D., *n* = 35). The mean Fe isotope compositions of international rock standards BIR-1 (Icelandic basalt) and Nod-PI (Pacific ferromanganese nodule) were: BIR-1, $\delta^{57}Fe$ = 0.082 ± 0.01‰; $\delta^{56}Fe$ = 0.062 ± 0.01‰ (2S.D., *n* = 6), Nod-PI $\delta^{57}Fe$ = -0.837 ± 0.02‰; $\delta^{56}Fe$ = -0.569 ± 0.03‰ (2S.D., *n* = 7). Iron yields were quantitative and chemistry blanks were <0.5ng Fe, negligible compared to the quantities of sample Fe (>300μg) processed.

The Pb isotope compositions were determined on bulk-rock powders by wet chemistry and a Nu Plasma 500 HR multiple-collector inductively coupled plasma mass spectrometer using Tl doping and sample–standard bracketing (Albarede et al., 2004) at the Ecole Normale Supérieure in Lyon. The whole-rock powders were leached in hot 6M HCl, including multiple ultrasonicating steps, prior to attack in a 3:1:0.5 mixture of double-distilled concentrated HF, HNO_3, and $HClO_4$. After fuming with double-distilled concentrated $HClO_4$ to eliminate fluorides from the sample digestion procedure, the samples were taken up in 6M HCl, placed on a hot plate until in complete solution, and evaporated to dryness. Lead was separated by ion-exchange chromatography on 0.5 ml columns filled with Bio-Rad AG1-X8 (100–200 mesh) resin using 1M HBr to elute the sample matrix and 6M HCl to collect the Pb. The total procedural Pb blank was < 20 pg. The NIST 981 Pb standard and the values of Eisele et al. (2003) were used for bracketing the unknowns (every two samples), and added Tl was used to monitor and correct for instrumental mass bias. The external reproducibility, estimated from the repeated NIST 981 measurements, are 100-200 ppm (or 0.01-0.02 %) for ratios based on 204 ($^{206}Pb/^{204}Pb$, $^{207}Pb/^{204}Pb$, $^{208}Pb/^{204}Pb$) and 50 ppm (or 0.005 %) for $^{207}Pb/^{206}Pb$, $^{208}Pb/^{206}Pb$, and $^{207}Pb/^{208}Pb$.

The Re–Os methodology for the analysis in Table DR4 followed techniques described in Bezard et al. (2015). An olivine separate from a harzburgite fragment shown in Fig. 1 was spiked for Re and Os and digested in inverse aqua regia (8 ml 16M HNO_3, 4 ml 12M HCl) by Carius tube dissolution followed by solvent extraction using the methods of Shirey and Walker (1995) and Cohen and Waters (1996). Rhenium was purified following Os extraction using anion exchange chromatography (Lambert et al., 1998) after back extraction in isoamylol. The osmium isotope composition was analysed in negative ion mode on a Thermo-Finnigan Triton at Macquarie University. The Os was loaded onto a Pt filament and analysed using by peak hopping for 200 ratios. Rhenium was determined using a quadrupole Agilent 7500 inductively coupled plasma mass spectrometer. A Re standard solution was analysed to monitor drift and fractionation. The sample was blank-corrected using 1 pg Re and 1.15 pg Os with a $^{187}Os/^{188}Os$ ratio of 0.164. Whole-rock standard (WPR-1; n=3) values in this laboratory average 10.53 ppb Re and 16.66 ppb Os with a $^{187}Os/^{188}Os$ ratio of 0.14466±0.00082, reproducing accepted values (e.g., Cohen and Waters, 1996). Further discussion of standard results and reproducibility is available in Day et al. (2015).

Host-melt – xenolith diffusion

When plotted against the reciprocal of their elemental composition, there is no simple correlation for either δ^7Li or $\delta^{57}Fe$ as would be expected from diffusive interaction between the host magma and xenoliths (Fig. DR1).

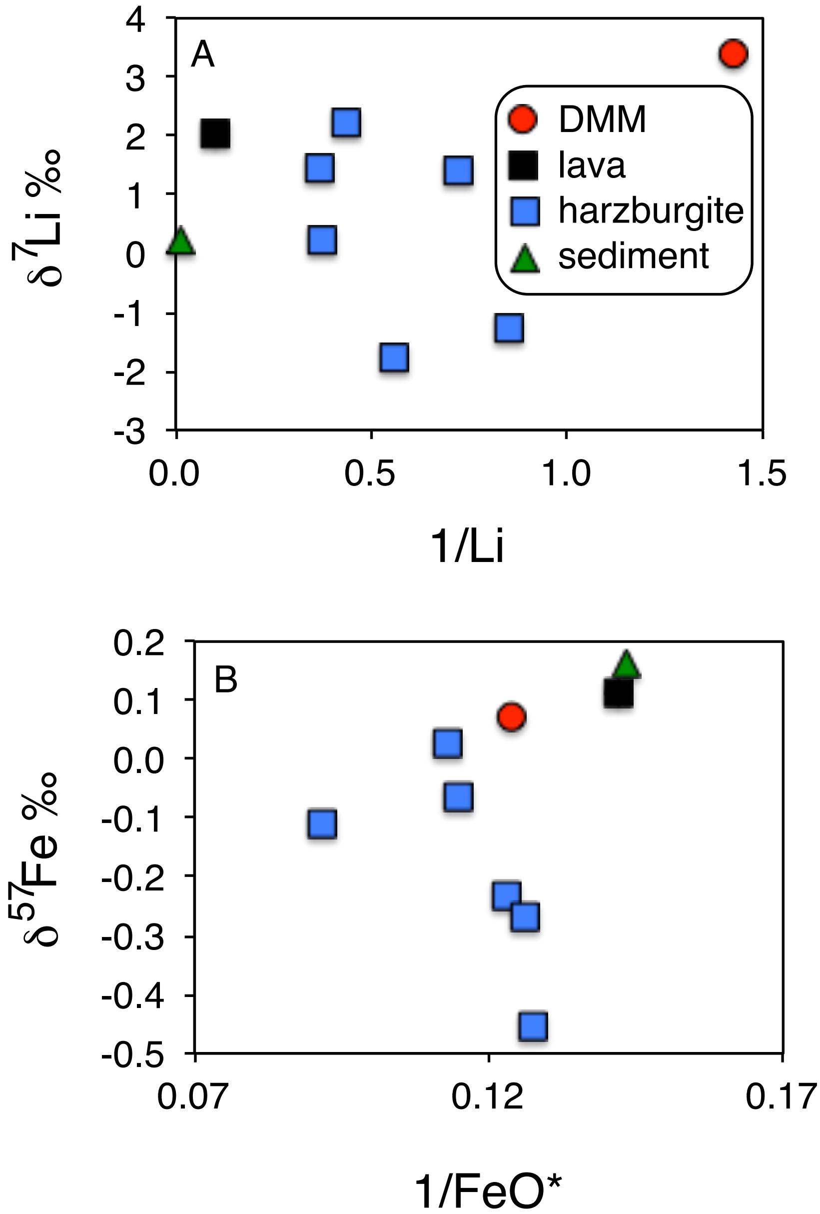

Figure DR1. Isotope – element systematics in Batan xenoliths. A: Plot of δ^7Li versus 1/Li and B: δ^{57}Fe versus 1/FeO* showing that there is no simple correlation as would be expected from diffusive interaction with the mantle wedge or host magma.

Li-Fe isotopic fluid-mantle wedge mixing models

Mixing models between a slab fluid and DMM end-members (δ^{57}Fe = 0.04 ‰; Williams and Bizimis 2016 and references therein) were constructed in order to evaluate if the Fe-Li stable isotope relationships (Fig. DR2) could be explained by the simple addition of an isotopically light fluid to the mantle wedge. In the absence of a direct proxy, the slab fluid component was approximated using Fe and Li concentration and isotopic data for high-temperature hydrothermal fluids vents (Fe isotopes: Rouxel et al., 2008, δ^{57}Fe = -2.67 ‰, [Fe] = 3105 µM; Li isotopes: Chan et al., 1993 δ^7Li = -6.8 ‰, [Li] = 1421 µM). The slab fluid - mantle wedge mixing model defines a strongly curved line on Fig. DR2, as a result of the extreme contrast in Li/Fe ratios between the fluid and mantle wedge. The contrast between the strong curvature of the mixing line and the broad linear array of the samples serves to demonstrate that simple binary mixing cannot be the dominant process in controlling the Li and Fe isotope systematics of the Batan xenoliths.

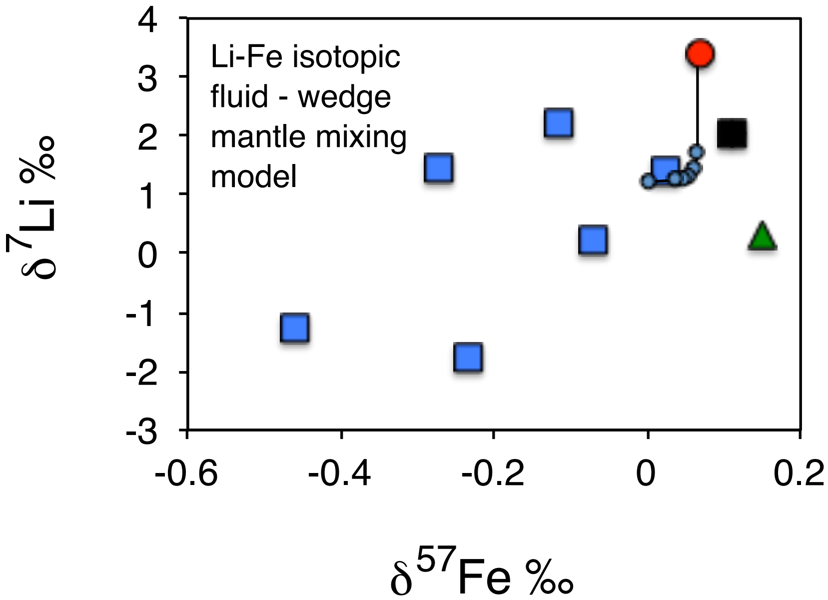

Figure DR2. Plot of δ^7Li versus δ^{57}Fe showing weak positive correlation. Fluid – wedge mixing model is strongly curved relative to the data and cannot reproduce the extent of stable isotope fractionation (marks along curve indicate 10% increments of fluid addition).

References

Albarede, F., Telouk, P., Blichert-Toft, J., Boyet, M., Agranier, A., and Nelson, B.K., 2004, Precise and accurate isotopic measurements using multiple-collector ICPMS: Geochimica et Cosmochimica Acta, v. 68, p. 2725–2744.

Bezard, R., Schaefer, B., Turner, S., Davidson, J.P., and Selby, D., 2015, Lower crustal assimilation in oceanic arcs: insights from an Osmium isotope study of the Lesser Antilles: Geochimica et Cosmochimica Acta, v. 150, p. 330-344.

Chan, L.H., Edmond, J.M., and Thompson, G., 1993, A lithium isotope study of hot springs and metabasalts from mid-ocean ridge hydrothermal systems: Journal of Geophysical Research, v. 98, p. 9653-9659.

Chaussidon, M., and Marty, B., 1995, Primitive boron isotope composition of the mantle. Science, v. 269, p. 383– 386.

Cohen, A.S., and Waters, F.G., 1996, Separation of osmium from geological materials by solvent extraction for analysis by thermal ionisation mass spectrometry. Analytica Chimica Acta, v. 332, p. 269–275.

Day, J.M.D., Waters, C.L., Schaefer, B.F., Walker, R.J., and Turner, S., 2015, Use of hydrofluoric acid desilicification in the determination of highly siderophile element abundances and Re-Os isotope systematics in mafic-ultramafic rocks: Geostandards and Geoanalytical Research, v. 39, p. 17-30.

Eisele, J., Abouchami, W., Galer, S.J., and Hofmann, A.W., 2003, The 320 kyr Pb isotope evolution of Mauna Kea lavas recorded in the HSDP-2 drill core: Geochemistry, Geophysics, Geosystems, v. 4, doi:10.1029/2002GC000339.

Lambert, D.D., Foster, J.G., Frick, L.R., Hoatson, D.M., Purvis, A.C., 1998, Application of the Re-Os isotopic system to the study of Precambrian magmatic sulfide deposits of Western Australia: Australian Journal of Earth Sciences, v. 45, p. 265–284.

Piazolo, S., Bestmann, M., Spiers, C., and Prior, D.J., 2006, Temperature dependent grain boundary migration mechanisms: Insights from in-situ experiments: Tectonophysics, v. 427, p. 55-71.

Rouxel, O., Shanks, W.C., Bach, W. and Edwards, K.J., 2008, Integrated Fe-and S-isotope study of seafloor hydrothermal vents at East Pacific Rise 9–10 N: Chemical Geology, v. 252, p. 214-227.

Rudnick, R.L., Tomascak, P.B., Heather, B.N., and Gardner, L.R., 2004, Extreme lithium isotopic fractionation during continental weathering revealed in saprolites from South Carolina: Chemical Geology, v. 212, p. 45–57.

Salters, V.J.M., and Stracke, A., 2004, Composition of the depleted mantle: Geochemistry, Geophysics, Geosystems, v. 5, doi:10.1029/2003GC000597.

Shirey, S.B., Walker, R.J., 1998, The Re-Os isotope system in cosmochemistry and high-temperature geochemistry: Annual Review of Earth and Planetary Sciences, v. 26, p. 423-500.

Stracke, A., Bizimis, M., and Salters, V.J.M., 2003, Recycling oceanic crust: quantitative constraints: Geochemistry, Geophysics, Geosystems, v. 4, doi:10.1029/2001GC000223.

Tonarini, S., Pennisi, M., and Leeman, W.P., 1997, Precise boron isotopic analysis of complex silicate (rock) samples using alkali carbonate fusion and ion exchange separation: Chemical Geology, v. 142, p. 129-137.

Turner, S., Caulfield, J., Turner, M., van Keken, P., Maury, R., Sandiford, M., and Prouteau, G., 2012, Recent contribution of sediments and fluids to the mantle's volatile budget: Nature Geoscience, v. 5, p. 50–54.

Williams, H., and Bizimis, M., 2014, Iron isotope tracing of mantle heterogeneity within the source regions of oceanic basalts: Earth and Planetary Science Letters, v. 404, p. 396–407.

Figure DR1

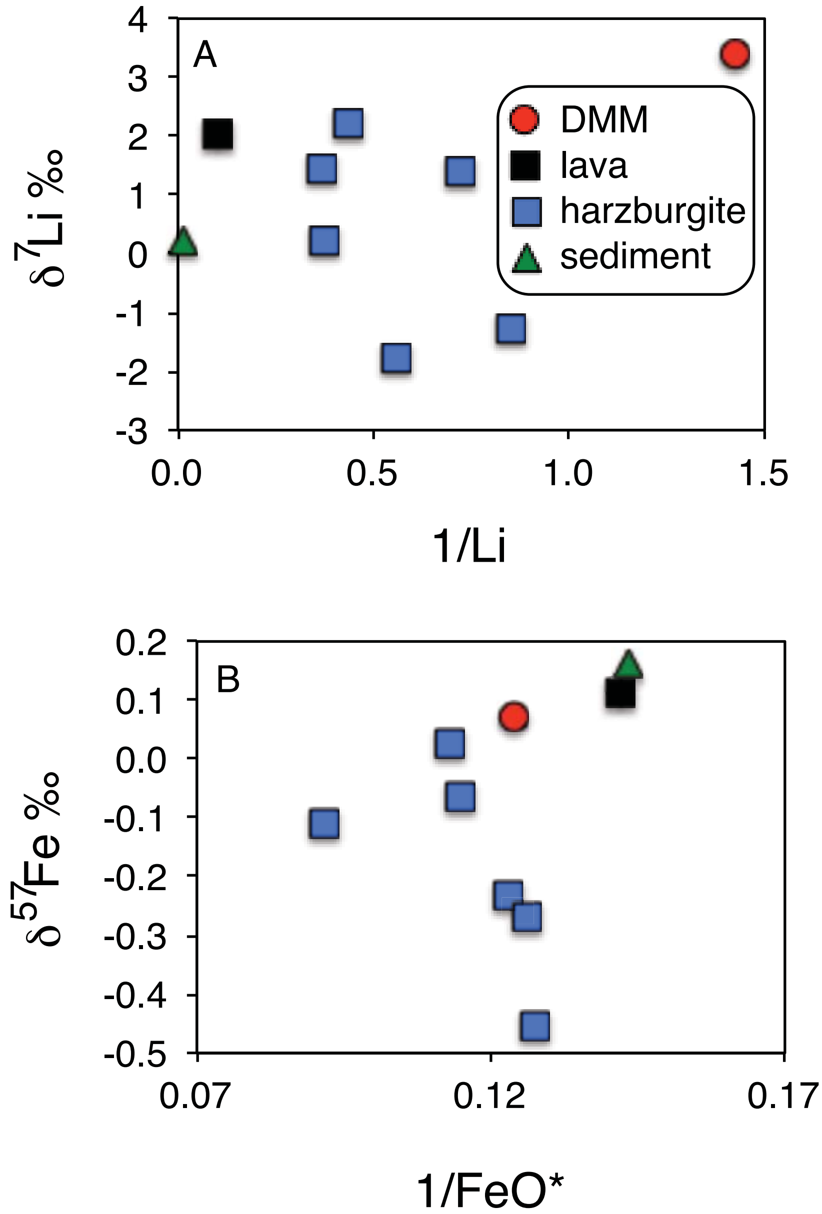
A
4
3
2
1
0
-1
-2
-3
0.0
0.5
1.0
1.5
1/Li
δ⁷Li ‰
DMM
lava
harzburgite
sediment
B
0.2
0.1
0.0
-0.1
-0.2
-0.3
-0.4
-0.5
0.07
0.12
0.17
1/FeO*
δ⁵⁷Fe ‰

Figure DR2

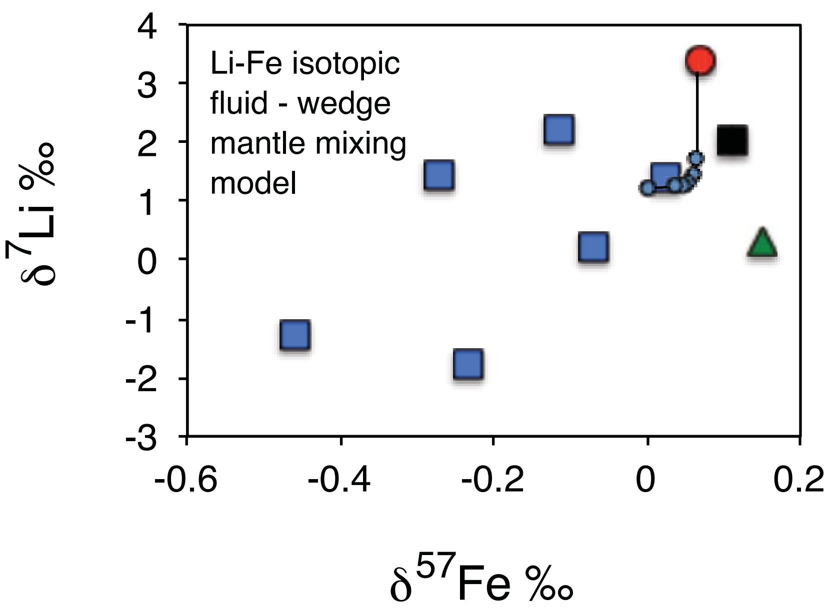

Li-Fe isotopic fluid - wedge mantle mixing model
δ⁷Li ‰
δ⁵⁷Fe ‰
4
3
2
1
0
-1
-2
-3
-0.6
-0.4
-0.2
0
0.2

Table DR1. Elemental and isotope compositions of the Batan Island host lava, mantle xenoliths, sediment and unmodified mantle

Sample #	Rock Type	B (ppm)	$\delta^{11}B$ ‰	Li (ppm)	$\delta^{7}Li$ ‰	FeO*	$\delta^{57}Fe$ ‰	Pb (ppm)	$^{206}Pb/^{204}Pb$	$^{207}Pb/^{204}Pb$	$^{208}Pb/^{204}Pb$	$^{87}Sr/^{86}Sr$
Song 24b	host lava	30.5	-5.65	9.43	2.01	7.03	0.11	13.64	18.435	15.620	38.749	*0.704450*
Song 24b	harzburgite	n/d	n/d	1.77	2.22	8.11	-0.11	0.73	18.384	15.602	38.658	*0.704512*
Song 24a	harzburgite	n/d	n/d	2.29	0.19	10.89	-0.07	0.26	18.431	15.699	38.477	*0.706661*
Song 3a	harzburgite	5.2	n/d	2.65	-1.30	8.69	-0.46	0.49	18.451	15.631	38.724	*0.704685*
Basco 17b	harzburgite	n/d	n/d	1.17	1.42	7.84	-0.27	0.15	18.374	15.628	38.640	*0.704875*
Balu 8	harzburgite	3.2	n/d	2.72	-1.78	7.92	-0.23	0.53	18.496	15.722	38.501	*0.707751*
B103	harzburgite	n/d	n/d	1.38	1.38	8.83	0.03	0.39	n/d	n/d	n/d	*0.704880*
RC17-159	sediment	n/d	-0.5	55.3	0.22	6.97	0.16†	24.20	18.868	15.682	38.276	0.712070
DMM	lherzolite	0.06	-5	0.7	3.4	8.07	0.07	0.023	18.018	15.486	37.903	0.703131

Depleted MORB mantle (DMM) based on Salters and Stracke (2004); Chaussidon and Marty (1995), Stracke et al. (2003); Elliott et al. (2004) and Williams and Bizimis (2014)

*total iron in wt. %; n/d = not determined, †estimated terigenous composition based on MORB

Sr isotope data in italics taken from Turner et al. (2012)

Table DR2. Representative major element analyses of minerals within the xenolith and host lava shown in Fig. 2, plus the groundmass of the lava

Component	harzburgite	harzburgite	harzburgite	harzburgite	hornblendite	gabbro	gabbro	host lava	host lava	host lava	host lava
Component	olivine	orthopyroxene	clinopyroxene	Cr-spinel	pargasite	pargasite	plagioclase	orthopyroxene	clinopyroxene	plagioclase	groundmass
SiO_2 (wt. %)	39.33	56.44	52.18	0.04	40.82	40.53	44.50	54.02	50.39	48.21	58.53
TiO_2	0.00	0.04	0.20	0.00	1.97	2.20	0.00	0.26	0.48	0.00	0.22
Al_2O_3	0.00	1.11	2.49	25.16	13.65	13.52	34.40	1.58	3.79	32.57	20.29
FeO	17.27	11.46	4.33	19.64	5.57	6.27	0.57	17.51	4.53	0.75	4.02
Cr_2O_3	0.02	0.07	0.49	41.71	0.00	0.00	0.00	0.00	0.00	0.00	0.00
Fe_2O_3	0.00	0.00	0.48	0.00	6.18	5.47	0.00	0.20	3.80	0.00	0.00
MnO	0.39	0.38	0.17	0.07	0.14	0.14	0.00	0.48	0.19	0.00	0.12
MgO	43.03	30.28	15.85	13.22	15.11	14.96	0.03	24.92	15.69	0.06	2.32
CaO	0.12	1.18	22.70	0.00	12.38	12.40	19.10	1.89	21.03	16.55	8.37
Na_2O	0.03	0.01	0.26	0.00	2.36	2.14	0.76	0.00	0.22	2.39	4.83
K_2O	0.00	0.00	0.01	0.00	0.97	1.17	0.03	0.00	0.00	0.08	1.15
NiO	0.30	0.05	0.00	0.12	0.00	0.00	0.00	0.00	0.00	0.00	0.00
Total	100.49	101.02	99.16	99.96	99.15	98.80	99.39	100.86	100.12	100.61	99.85

Table DR3. Representative trace element analyses of minerals within the xenolith shown in Fig. 2

Component Mineral	harzburgite olivine	harzburgite orthopyroxene	harzburgite clinopyroxene	hornblendite hornblende	gabbro hornblende	gabbro plagioclase
Li (ppm)	3.2	1.3	1.67	1.3	1.18	0.48
Be	<0.073	<0.063	0.109	0.412	0.573	0.38
B	<1	5.12	4.75	5.39	3.17	4.42
Sc	7.03	12.09	83.3	100.28	106.18	1.618
V	3	34.25	182.46	500.03	572.27	7.98
Cr	3	1189.47	6616.84	230.16	188.82	<0.99
Co	186	61.09	24.5	50.58	56.02	0.827
Ni	2210	544.43	299.72	303.45	205	1.28
Cu	5.92	1.25	5.14	2.68	2.64	2.69
Zn	157	104.59	26.95	47.61	58.07	5.67
Ga	0.3	2.209	3.61	27.91	26.44	23.44
Rb	0.13	<0.055	0.079	9.44	7.37	3.43
Sr	0.091	0.123	49.81	393.66	362.17	1135.88
Y	0.071	0.824	10.95	17.71	16.92	0.547
Zr	0.17	0.642	18.32	50.47	39.11	4.77
Nb	0.1	<0.0086	0.0219	3.25	2.29	0.322
Cs	0.07	<0.0231	<0.029	0.217	0.028	0.261
Ba	0.5	<0.0178	0.137	253.4	266.26	69.92
La	0.06	<0.0105	2.001	4.63	5.03	2.91
Ce	0.05	0.0304	9.01	17.35	18.28	5.47
Pr	0.05	<0.0041	1.942	3.21	3.13	0.613
Nd	0.32	0.088	12	18.02	16.61	1.88
Sm	0.3	0.053	3.2	4.96	4.42	0.355
Eu	0.09	0.0139	0.738	1.383	1.4	0.286
Gd	0.3	0.094	2.64	4.18	3.76	0.142
Tb	0.04	0.0156	0.354	0.599	0.537	0.0165
Dy	0.3	0.121	2.3	3.74	3.25	0.11
Ho	0.05	0.0408	0.427	0.737	0.704	0.0229
Er	0.2	0.129	1.183	1.817	1.79	0.043
Tm	0.06	0.0283	0.165	0.241	0.229	<0.0093
Yb	0.34	0.161	0.93	1.488	1.479	0.038
Lu	0.06	0.0192	0.133	0.228	0.206	0.0162
Hf	0.17	0.038	1.422	2.098	1.539	0.103
Ta	<0.07	<0.0054	0.0059	0.1402	0.0967	0.0087
Pb	0.21	<0.033	0.12	1.618	1.425	1.465
Th	0.05	<0.0065	0.0789	0.577	0.322	0.53
U	0.05	<0.0058	0.01	0.1093	0.0374	0.112

Table DR4. Re-Os isotope data for olivine from a harzburgite fragment

Re (ppb)	2σ	Os (ppb)	2σ	$^{187}Re/^{188}Os$	2σ	$^{187}Os/^{188}Os$	2σ
0.944	0.014	1.5713	0.0009	22.890	0.144	0.12660	0.0001